

Neutron-proton asymmetry dependence of nuclear temperature with intermediate mass fragments

X. Liu(刘星泉),^{1,2} H. Zheng(郑华),³ R. Wada,^{4,5} W. Lin(林炜平),^{1,*} M. Huang(黄美容),⁶ P. Ren(任培培),¹ G. Qu(曲国峰),¹ J. Han(韩纪锋),¹ S. Kowalski,⁷
T. Keutgen,⁸ K. Hagel,⁴ M. Barbui,⁴ A. Bonasera,^{4,9} and J.B. Natowitz⁴

¹*Key Laboratory of Radiation Physics and Technology of the Ministry of Education,
Institute of Nuclear Science and Technology,
Sichuan University, Chengdu 610064, China*

²*Institute of Modern Physics, Chinese Academy of Sciences, Lanzhou, 730000, China*

³*School of Physics and Information Technology,
Shaanxi Normal University, Xi'an 710119, China*

⁴*Cyclotron Institute, Texas A&M University, College Station, Texas 77843*

⁵*School of Physics, Henan Normal University, Xinxiang 453007, China*

⁶*College of Physics and Electronics information,
Inner Mongolia University for Nationalities, Tongliao, 028000, China*

⁷*Institute of Physics, Silesia University, Katowice, Poland.*

⁸*FNRS and IPN, Université Catholique de Louvain, B-1348 Louvain-Neuve, Belgium*

⁹*Laboratori Nazionali del Sud, INFN,
via Santa Sofia, 62, 95123 Catania, Italy*

(Dated: August 28, 2019)

Abstract

The dependence of the nuclear temperature on the source neutron-proton (N/Z) asymmetry is experimentally investigated with the intermediate mass fragments (IMFs) generated from 13 reaction systems with different N/Z asymmetries, ^{64}Zn on ^{112}Sn and ^{70}Zn , ^{64}Ni on $^{112,124}\text{Sn}$, $^{58,64}\text{Ni}$, ^{197}Au , ^{232}Th at 40 MeV/nucleon. The apparent source temperatures for these systems are determined from the measured IMFs yields from the intermediate velocity sources using eight carbon-related double isotope ratio thermometers. A rather weak N/Z asymmetry dependence of the source temperature is qualitatively inferred from the extracted N/Z asymmetry dependence of the apparent temperature and that of the relative temperature change by the sequential decay effects with the help of the theoretical simulations. The present result is compared with those from other available experiments.

* E-mail at: linwp1204@scu.edu.cn

1 I. INTRODUCTION

2 The neutron-proton (N/Z) asymmetry dependence of the nuclear caloric curve, namely
3 the dependence of the temperature relative to the excitation energy on the N/Z asymmetry
4 of the reaction system (or the fragmenting source), provides crucial information on the N/Z
5 asymmetry dependence of the nuclear forces, the properties of excited nuclei and the pos-
6 tulated nuclear liquid-gas phase transition [1–4]. However, large uncertainties in the N/Z
7 asymmetry dependence of the nuclear caloric curve still remain, due to the relatively scarce
8 experimental data and the conflicting conclusions drawn from the experiments and theoret-
9 ical studies. For the experimental studies on the N/Z asymmetry dependence of the nuclear
10 temperature, Sfienti *et al.* [5], Trautmann *et al.* [6] and Wuenschel *et al.* [7] found that the
11 experimentally extracted source temperatures show a rather weak dependence on the N/Z
12 asymmetry of the fragmenting source. In contrast, McIntosh *et al.* [8] found that the ex-
13 tracted temperatures are notably higher for relatively proton-richer systems than those for
14 neutron-richer systems. In theoretical works, some predicted that limiting temperatures, de-
15 fined as the plateau temperature of the caloric curve, are higher for neutron-poor systems [9],
16 whereas others made the opposite prediction [10–12]. These experimental and theoretical
17 ambiguities are attributed to various causes, such as the application of different thermome-
18 ters which may reflect different fragmentation mechanisms [8, 13–16], different modeling
19 assumptions in theoretical calculations among others [9]. To address these issues and pur-
20 sue a consistent description for the N/Z asymmetry dependence of the nuclear temperature,
21 further effort is still required in both experimental and theoretical studies.

22 Light charged particles (LCPs) have been the primary temperature probe in the previous
23 studies [17]. As intermediate mass fragments (IMFs) are copiously produced through the
24 multifragmentation process in intermediate heavy-ion collisions [18], they provide an addi-
25 tional opportunity to study the temperature behavior as well. We recently experimentally
26 extracted the temperature of the fragmenting source from the IMF isotope distributions
27 with a self-consistent method [19–23] and then studied the incident energy dependence of
28 the temperature [24]. These works provide us an opportunity to pursue the source N/Z
29 asymmetry dependence of the nuclear temperature using IMFs as a probe.

30 In this work, we use IMFs from 13 reaction systems with different N/Z asymmetries to
31 investigate the N/Z asymmetry dependence of the nuclear temperature. The double iso-

32 tope ratio thermometer [25] is adopted to extract the temperatures from the IMF isotope
 33 yields. As the measured isotope yields are perturbed by the sequential decay, it may result
 34 in a serious inaccuracy in the temperature determination using the double isotope ratio
 35 thermometer, even though the sequential decay effect has been considered in some extent
 36 [5, 26, 27]. Therefore, the experimentally inferred temperature from the double isotope ratio
 37 thermometer is called “apparent temperature”, whereas that before the sequential decays
 38 is called “real (source) temperature”. However, the double isotope ratio thermometer has
 39 been widely used to study thermodynamic properties of fragmenting sources, i.e., temper-
 40 ature as a function of excitation energy (caloric curve) [17, 26, 28, 29], N/Z asymmetry
 41 dependence [5, 6, 30, 31], and time evolution during the collisions [32]. These studies indi-
 42 cate that even though the temperature values (with or without sequential corrections) from
 43 different double isotope ratio thermometers are not always consistent, the double isotope
 44 ratio thermometer used as a relative thermometer could reflect the general behaviors of the
 45 nuclear temperature dependence on excitation energy, source N/Z asymmetry, time evolu-
 46 tion and among others qualitatively. Following the strategy of these previous works, the N/Z
 47 asymmetry dependence of the real source temperature is therefore studied using the double
 48 isotope ratio thermometer in this work. Theoretical model calculations are also performed
 49 to compare to the experimental results and provide insight into the sequential decay effect.
 50 This article is organized as follows. In Sec.II, we briefly describe the experiment and data
 51 analysis. In Sec.III, a description for the double isotope ratio formalism is given. In Sec.IV,
 52 the N/Z asymmetry dependence of the apparent temperature is determined. In Secs.V and
 53 VI, discussion and summary are given.

54 II. EXPERIMENT AND DATA ANALYSIS

55 1. EXPERIMENT

56 The experiment was performed at the K-500 superconducting cyclotron facility at Texas
 57 A&M University. $^{64,70}\text{Zn}$ and ^{64}Ni beams were used to irradiate $^{58,64}\text{Ni}$, $^{112,124}\text{Sn}$, ^{197}Au
 58 and ^{232}Th targets at 40 MeV/nucleon. 13 reaction systems, ^{64}Zn on ^{112}Sn and ^{70}Zn , ^{64}Ni
 59 on $^{112,124}\text{Sn}$, $^{58,64}\text{Ni}$, ^{197}Au , ^{232}Th , were analyzed in this work. The physical views of the
 60 detector setup used in the experiment are presented in Fig. 1. IMFs were detected by a

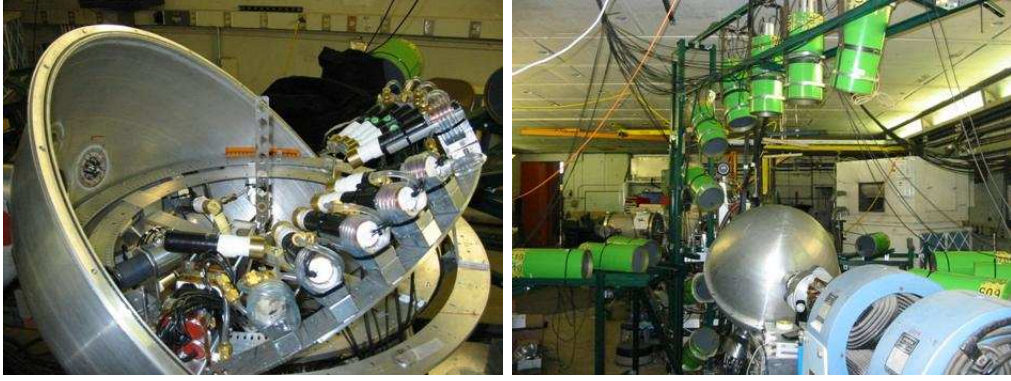


FIG. 1. (color online) Physical views of the detector setup. Left: the IMF telescope and 16 CsI detectors were arranged around the target inside the spherical scattering chamber; Right: the 16 DEMON detectors for neutron measurement were arranged outside the chamber. The pictures were taken before the runs and the detector arrangements in the left figure are slightly different from the actual runs. Two figures have not been digitally altered.

61 detector telescope placed at 20° in the spherical scattering chamber (left of Fig. 1). The
 62 telescope consisted of four Si detectors. Each Si detector was $5\text{ cm} \times 5\text{ cm}$. The nominal
 63 thicknesses were 129, 300, 1000, 1000 μm , respectively. All four Si detectors were segmented
 64 into four sections and each quadrant had a 5° opening in the polar angle. During the
 65 experiment, the telescope signals were taken inclusively as the main trigger for all detected
 66 events. Typically 6 \sim 8 isotopes for atomic numbers as high as $Z = 18$ were clearly identified
 67 with energy thresholds of 4 \sim 10 MeV/nucleon, using the $\Delta E - E$ technique for any two
 68 consecutive detectors. Mass identification of the isotopes was made using a range-energy
 69 table [33]. Besides IMFs, the LCPs in coincidence with IMFs were also measured using
 70 16 single-crystal CsI(Tl) detectors of 3 cm length set around the target at angles between
 71 $\theta_{Lab} = 27^\circ$ and $\theta_{Lab} = 155^\circ$. Sixteen detectors of the Belgian-French neutron detector
 72 array DEMON (Detecteur Modulaire de Neutrons, right of Fig. 1) [34] outside the chamber
 73 were used to measure neutrons, covering polar angles of $15^\circ \leq \theta_{IMF-n} \leq 160^\circ$ between
 74 the telescope and the neutron detectors. Data analysis with these LCP and neutrons were
 75 presented in Refs. [20, 35]. In this article, we focus on the data analysis of the measured
 76 IMFs.

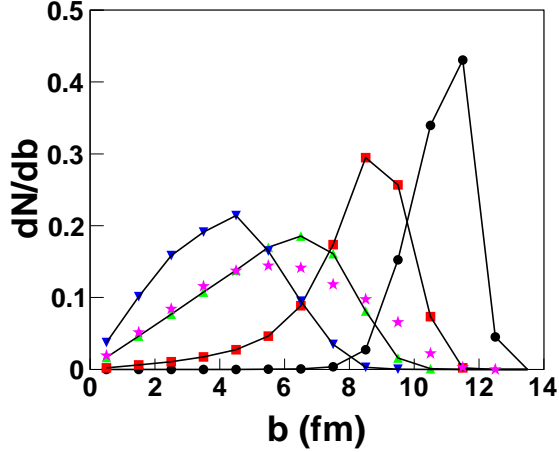


FIG. 2. (color online) Simulated impact parameter distributions for violent (downward triangles), semi-violent (upward triangles), semi-peripheral (squares) and peripheral (dots) collisions of $^{64}\text{Zn}+^{112}\text{Sn}$ at 40 MeV/nucleon. Stars indicate the events in which at least one IMF ($Z \geq 3$) is emitted at 15° - 25° . The summed distribution for a given event class is normalized to 1. The figure is taken from Ref. [39].

2. EVENT IDENTIFICATION

Since the IMFs were taken inclusively, the angle of the IMF telescope was set carefully to optimize the IMF yields. The consideration was that the angle should be small enough to ensure that sufficient IMF yields are obtained above the detector energy threshold, as well as large enough to minimize contributions from peripheral collisions. For this purpose, simulations of the antisymmetrized molecular dynamics model (AMD) [36] incorporating the statistical decay code GEMINI as an afterburner [37] (used in the previous work [38]) were performed. Fig. 2 presents the calculated impact parameter distributions for the system of $^{64}\text{Zn}+^{112}\text{Sn}$ at 40 MeV/nucleon. In this figure, the violence of the reaction for each event was determined in the same way as that in Ref. [38], in which the multiplicity of light particles, including neutrons, and the transverse energy of light charged particles were used. The resultant impact parameter distributions for each class of events are shown together with that of the events in which at least one IMF is emitted at the polar angles within 15° - 25° . As seen in the figure, the distribution of the events selected by this IMF trigger is similar to that of semi-violent collisions.

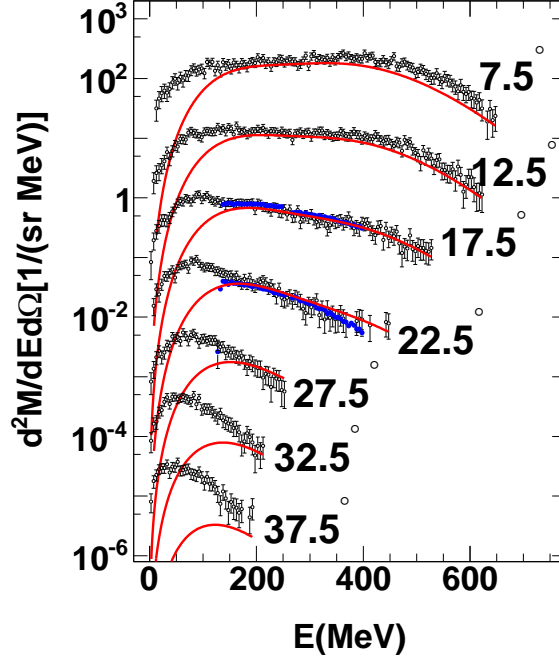


FIG. 3. (Color online) Experimental ^{16}O energy spectra for the system of $^{64}\text{Zn}+^{112}\text{Sn}$ at 40 MeV/nucleon (closed circles) are compared with those of AMD+GEMINI simulation (open circles). The spectra of the AMD+GEMINI simulation were obtained from the semi-violent collisions. The curves are the results of the moving source fit, for which the parameters were determined from the experimental spectra at 17.5° and 22.5° . Angles are given in the figure and the absolute Y scale is corresponding to the bottom spectra and the spectra are multiplied by a factor of 10 from the bottom to the top. The figure is taken from Ref. [39].

93 3. SOURCE CHARACTERIZATION AND MULTIPLICITY DETERMINATION

94 In order to further characterize the fragmenting source to isolate the reaction mechanisms
 95 involved in the reaction products, a moving source fit [40] was employed. In the moving
 96 source fit, the sources were classified as projectile-like (PLF), intermediate-velocity (IV)
 97 (also called as nucleon-nucleon-like (NN) [41]), and target-like (TLF) sources according to
 98 the source velocity. The isotope spectra of IMFs from 15° - 25° were fitted using a single
 99 IV source. Using a source with a smeared source velocity around half the beam velocity,
 100 the fitting parameters were first determined from the spectrum summed over all isotopes
 101 for a given Z under an assumption of $A = 2Z$. Then all extracted parameters except the
 102 normalizing yield parameter were applied to the other individual isotopes with the same Z ,

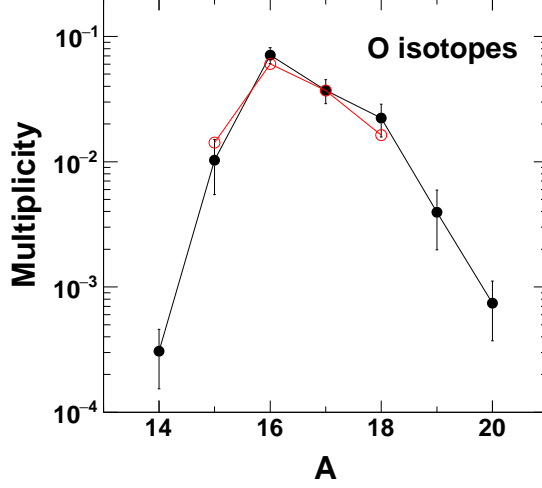


FIG. 4. (Color online) Oxygen isotope multiplicity distribution determined from the moving source fits for the spectra of $^{64}\text{Zn}+^{112}\text{Sn}$ at 40 MeV/nucleon at 17.5° and 22.5° (closed circles), together with those from the three-source moving source fits for the corresponding AMD+GEMINI spectra (open circles). See details about the experimental error evaluation in the text. Also note that no error is presented for the AMD+GEMINI case.

103 and the multiplicity for each given isotope was obtained as a parameter from the moving
 104 source fits. In Fig. 3, the experimental energy spectra of ^{16}O at 17.5° and 22.5° are presented
 105 by closed circles as an example and compared with those from the semi-violent collisions
 106 predicted by AMD+GEMINI simulations. The experimental spectra at 17.5° and 22.5°
 107 are reproduced reasonably by the AMD+GEMINI simulation. The experimental spectra at
 108 17.5° and 22.5° were fitted using a single IV source with the aid over the MINUIT program
 109 in the Cern ROOT library. Solid red curves correspond to the fit results. Good agreement
 110 between the experimental results (as well as those from the AMD+GEMINI simulation)
 111 and the fits at 17.5° and 22.5° is obtained, although significant deviation appears on the
 112 lower energy part of the spectrum. This deviation is attributed to the TLF component.
 113 The TLF component could not be fully measured in this experiment due to the high energy
 114 thresholds for IMFs. We also note that a small enhancement in the AMD+GEMINI spectra
 115 above the moving source fit at forward angles which is attributed to the PLF component. In
 116 Fig. 4, the Oxygen isotope multiplicities of the IV source component determined from the
 117 single-source moving source fits are presented with the error bars which are described below.
 118 The corresponding results from the three-source moving source fits for the AMD+GEMINI

119 spectra are also plotted for comparison. The close agreement between both results suggests
 120 a good assumption of single-source fit to the present experimental IMF spectra.

121 The errors of the isotope yields from the moving source fits were evaluated by performing
 122 different optimizations with different initial values within a wide range, including source
 123 velocity, energy slope and among others, rather than the errors given by the MINUIT from
 124 the fits, because there were many local minima for the multiple parameter fits. Rather
 125 large errors (around $\pm 10\%$) were assigned for the multiplicity of the IV source for IMFs,
 126 originating from the source fit. Similar moving source fits were also applied to the energy
 127 spectra of LCPs and neutrons. The extracted IV-source multiplicities of neutrons, LCPs and
 128 IMFs for all 13 reactions are given in SUPPLEMENTAL MATERIAL of this article. Only
 129 the multiplicities of the fragments emitting from the IV source were used in the following
 130 investigation of the source N/Z asymmetry dependence of the nuclear temperature.

131 III. DOUBLE ISOTOPE RATIO THERMOMETER FORMALISM

132 The double isotope ratio thermometer was first proposed by Albergo *et al.* [25]. Under
 133 the assumption that thermal equilibrium may be established between free nucleons and
 134 composite fragments contained within a certain freezeout volume V and a temperature T ,
 135 the density of an isotope with A nucleons and Z protons (A, Z) may be expressed as

$$\rho(A, Z) = \frac{N(A, Z)}{V} = \frac{A^{3/2} \cdot \omega(A, Z)}{\lambda_T^3} \cdot \exp\left[\frac{\mu(A, Z)}{T}\right], \quad (1)$$

136 where $N(A, Z)$ is the number of isotope (A, Z) within the volume V ; $\lambda_T = h/(2\pi m_0 T)^{1/2}$
 137 is the thermal nucleon wave-length, where m_0 is the nucleon mass; $\omega(A, Z)$ is the internal
 138 partition function of the isotope (A, Z) and related to the ground- and excited-state spins
 139 (practically, $\omega(A, Z)$ is limited to that at the ground state [25]); $\mu(A, Z)$ is the chemical
 140 potential of the isotope (A, Z). In chemical equilibrium, $\mu(A, Z)$ is expressed as

$$\mu(A, Z) = Z\mu_p + (A - Z)\mu_n + B(A, Z), \quad (2)$$

141 where $B(A, Z)$ is the binding energy of the isotope (A, Z). μ_p and μ_n are the chemical
 142 potentials of free protons and free neutrons, respectively. Calculating the densities of free
 143 protons and neutrons, ρ_p and ρ_n , in the same volume using Eqs. 1 and 2, performing

144 transforms to obtain μ_p and μ_n , and then inserting μ_p and μ_n back into Eq. 1, one obtains,

$$\rho(A, Z) = \frac{N(A, Z)}{V} = \frac{A^{3/2} \cdot \omega(A, Z) \cdot \lambda_T^{3(A-1)}}{(2s_p + 1)^Z \cdot (2s_n + 1)^{A-Z}} \cdot \rho_p^Z \cdot \rho_n^{A-Z} \exp \left[\frac{B(A, Z)}{T} \right], \quad (3)$$

145 where s_p and s_n are the spins of the free proton and neutron, respectively. The ratio between
146 the measured yields of two different isotopes is then

$$\frac{Y(A, Z)}{Y(A', Z')} = \frac{\rho(A, Z)}{\rho(A', Z')} = \left(\frac{A}{A'} \right)^{3/2} \left(\frac{\lambda_T^3}{2} \right)^{A-A'} \frac{\omega(A, Z)}{\omega(A', Z')} \rho_p^{(Z-Z')} \rho_n^{(A-Z)-(A'-Z')} \exp \left[\frac{B(A, Z) - B(A', Z')}{T} \right], \quad (4)$$

147 The free proton density can be calculated from the yield ratio of two fragments with only
148 one proton difference, such as (A, Z) and $(A + 1, Z + 1)$,

$$\rho_p = C \cdot \left(\frac{A}{A+1} \cdot T \right)^{3/2} \frac{\omega(A, Z)}{\omega(A+1, Z+1)} \cdot \exp \left[\frac{B(A, Z) - B(A+1, Z+1)}{T} \right] \cdot \frac{Y(A+1, Z+1)}{Y(A, Z)}, \quad (5)$$

149 where C is the constant related to the unit conversion. Analogously, the free neutron density
150 is calculated from the yield ratio of two fragments with only one neutron difference, such as
151 (A, Z) and $(A + 1, Z)$,

$$\rho_n = C \cdot \left(\frac{A}{A+1} \cdot T \right)^{3/2} \frac{\omega(A, Z)}{\omega(A+1, Z)} \cdot \exp \left[\frac{B(A, Z) - B(A+1, Z)}{T} \right] \cdot \frac{Y(A+1, Z)}{Y(A, Z)} \quad (6)$$

152 For a given temperature T , the same free proton (or neutron) density must be evaluated
153 from Eq. 5 (or 6). Choosing two ratios with one proton (or neutron) excess, one can deduce
154 the relation between T and the experimental yield ratios as

$$T = \frac{\Delta B}{\ln(aR)}, \quad (7)$$

155 where $R = (Y_1/Y_2)/(Y_3/Y_4)$ is the double isotope yield ratio of the ground states for isotope
156 pairs (1, 2) and (3, 4). In this work, the experimental (1, 2) and (3, 4) ratios with same one-
157 neutron excess are adopted. ΔB is the binding energy difference, $\Delta B = (B_1 - B_2) - (B_3 - B_4)$.
158 a is the statistical weighting factor and is defined as

$$a = \frac{\omega_3/\omega_4}{\omega_1/\omega_2} \left[\frac{A_3/A_4}{A_1/A_2} \right]^{1.5}, \quad (8)$$

159 where $\omega_i = 2S_i + 1$ and S_i is the ground state spin of the i th isotope and A_i is the mass
160 number of the i th isotope. In the actual temperature determination, isotope pairs with large

161 ΔB values are recommended [42]. Following Ref. [42], the IMF temperatures in this work
 162 are therefore determined using eight carbon-related isotope ratios with $\Delta B > 10$ MeV. The
 163 ratios used for constructing the thermometers and their associated ΔB and a values are
 164 listed in Table I.

TABLE I. List of the parameters for the eight carbon-related thermometers used in the present work.

ID	Isotope ratio	ΔB (MeV)	a
1	${}^6,7\text{Li}/{}^{11,12}\text{C}$	11.47	5.90
2	${}^7,8\text{Li}/{}^{11,12}\text{C}$	16.69	5.36
3	${}^9,10\text{Be}/{}^{11,12}\text{C}$	11.91	1.03
4	${}^{11,12}\text{B}/{}^{11,12}\text{C}$	15.35	3.00
5	${}^{12,13}\text{B}/{}^{11,12}\text{C}$	13.84	5.28
6	${}^{12,13}\text{C}/{}^{11,12}\text{C}$	13.77	7.92
7	${}^{13,14}\text{C}/{}^{11,12}\text{C}$	10.54	1.96
8	${}^{15,16}\text{N}/{}^{11,12}\text{C}$	16.23	9.67

165 IV. RESULTS- N/Z ASYMMETRY DEPENDENCE OF APPARENT TEMPERA- 166 TURE

167 The resultant apparent temperature values from the eight thermometers are plotted in
 168 Fig. 5 as a function of the source N/Z asymmetry, $\delta_{IV} = (N_{IV} - Z_{IV})/A_{IV}$, where N_{IV} ,
 169 Z_{IV} and A_{IV} are the neutron, proton and mass of the fragmenting source calculated from
 170 summing over the experimentally measured IV component yields of neutrons, LCPs and
 171 IMFs with Z up to 18. Errors shown in the figure are calculated from the isotope multiplicity
 172 errors. Note again that as the experimental yields which result from the sequential decay
 173 are used in Eq. 7, the calculated temperatures in this section are the apparent temperatures.
 174 The extracted apparent temperatures from all eight thermometers shown in the figure exhibit
 175 almost no dependence on δ_{IV} . A global fit to the eight T_{app} vs δ_{IV} plots with linear functions
 176 with one common slope k_{app} and individual intercepts is performed. k_{app} in the fit reflects the

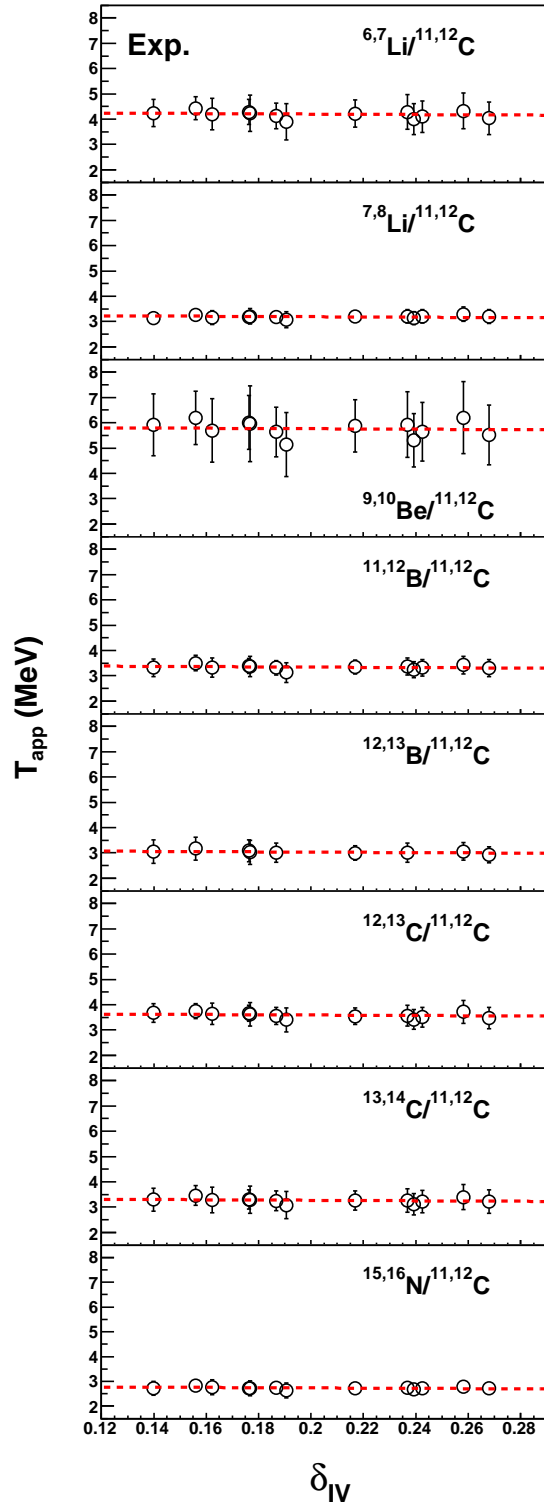


FIG. 5. (color online) Apparent temperatures T_{app} from the eight carbon-related double isotope ratio thermometers as a function of source N/Z asymmetry δ_{IV} . Red dashed lines are the global fits with linear functions with one common slope k_{app} and different intercepts.

177 average trend of the apparent temperature as δ_{IV} increases, whereas the individual intercepts
 178 are sensitive to the extracted values of apparent temperature. A common slope, $k_{app} =$
 179 -0.5 ± 0.1 MeV is obtained, where the error is the fitting error. The small k_{app} value indicates
 180 that the apparent temperature decreases weakly as the source N/Z asymmetry increases,
 181 that is, the apparent temperature decreases ~ 0.07 MeV on average as δ_{IV} increases from
 182 0.14 to 0.27 for the present source N/Z asymmetry region. Different intercept values of ~ 3 -6
 183 MeV is also obtained for the different thermometers in contrast.

184 V. DISCUSSION

185 1. TEMPERATURE FROM AMD SIMULATIONS FOR $^{64}\text{Zn}+^{112}\text{Sn}$

186 Taking the reaction system of $^{64}\text{Zn}+^{112}\text{Sn}$ as an example, the apparent temperature val-
 187 ues from the eight thermometers are compared in Fig. 6, together with those from the
 188 AMD+GEMINI simulation, $T_{app,AMD}$. The AMD+GEMINI events with an impact pa-
 189 rameter range of 0-8 fm are used in this analysis. An approximated isotope selection for
 190 characterizing the IV source, $E_{lab}/A > 5$ MeV and $5^\circ < \theta_{lab} < 25^\circ$, is applied to these
 191 events. This selection method has been verified in our previous work [20]. Errors of the
 192 apparent temperature values from the AMD+GEMINI simulated events, which are within
 193 symbols, are evaluated from the statistical errors of the generated events. In the figure,
 194 the experimental and theoretical apparent temperatures are rather consistent, though a few
 195 simulated values are out of the experimental error bars. Both show a significant apparent
 196 temperature fluctuation of ~ 3 -6 MeV, which corresponds to fluctuations in the heights of
 197 the horizontal dashed lines at a given value of δ_{IV} in Fig 5.

200 In Fig. 7, the extracted real temperature, T_{AMD} , from the primary isotope yields of
 201 the AMD simulations for the $^{64}\text{Zn}+^{112}\text{Sn}$ system, the above AMD apparent temperature,
 202 $T_{app,AMD}$, and the difference between these two temperatures, ΔT ($\Delta T = T_{app,AMD} - T_{AMD}$),
 203 are shown for the different thermometers. The same event and isotope selections as those of
 204 the AMD+GEMINI are applied to the AMD events [20], though this is only approximately
 205 true for the primary fragments. The extracted source temperature for the eight thermome-
 206 ters from the primary yields varies from ~ 3.5 MeV to ~ 7 MeV shown by solid circles in the
 207 figure. This result reveals an incredibility for the double isotope ratio thermometers that

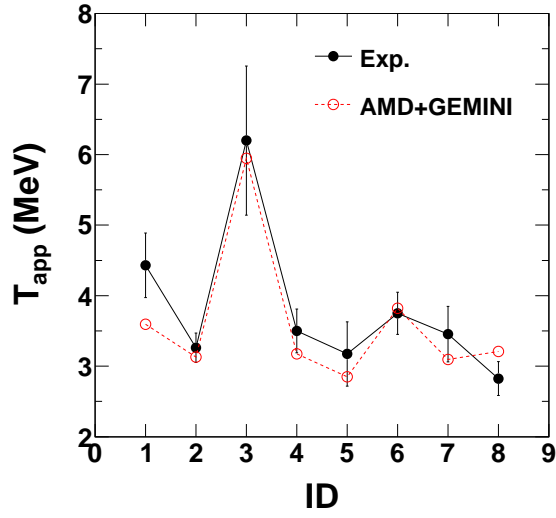


FIG. 6. (color online) Apparent temperatures from the eight carbon-related double isotope ratio thermometers from the $^{64}\text{Zn}+^{112}\text{Sn}$ system as a function of the thermometer ID given in TABLE I. Dots and circles are those from the experiment and the AMD+GEMINI simulations, respectively. Lines are for the guide of eyes.

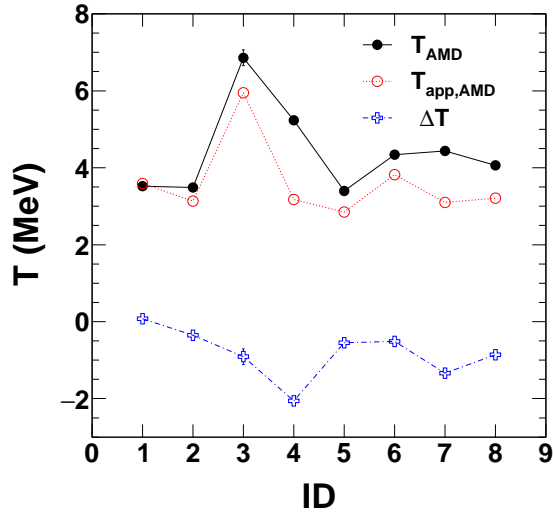


FIG. 7. (color online) Temperatures from the eight carbon-related double isotope ratio thermometers from the primary and secondary isotope yields, T_{AMD} and $T_{app,AMD}$, of the $^{64}\text{Zn}+^{112}\text{Sn}$ system, together with the relative temperature change, ΔT , between $T_{app,AMD}$ and T_{AMD} , as a function of the thermometer ID given in TABLE I. Lines are for the guide of eyes.

208 it does not yield a common temperature for a given fragmenting system. The inconsistent
 209 values of the real source temperature have also been commonly observed in the LCP temper-
 210 ature evaluation of the double isotope ratio thermometers after the quantitative sequential
 211 decay corrections [5, 26, 27]. This fact may be attributed to different reaction dynamics and
 212 fragment production mechanisms. The apparent temperature inherits this primary fluctua-
 213 tion, as indicated by the similar pattern of the T_{AMD} and $T_{app,AMD}$ values shown in Fig. 7.
 214 This is true for all other reactions in the AMD simulations discussed below. In contrast
 215 to the temperatures from the primary and secondary isotopes, the ΔT values for the eight
 216 thermometers show slightly smaller fluctuations from ~ -2 to ~ 0 MeV, reflecting a cancel-
 217 lation for the effects of the reaction dynamics and the fragment production mechanisms.
 218 The remaining ΔT fluctuation may be attributed to the nuclear structure information for
 219 individual isotopes in the de-excitation process, as pointed out in Ref. [43].

220 In the present work, instead of using the double isotope thermometer as an absolute ther-
 221 mometer, we use it as a relative thermometer and divide the N/Z asymmetry dependence
 222 of the real source temperature into two effects. One is the N/Z asymmetry dependence
 223 of the apparent temperature, which has been discussed above, and the other is that of the
 224 relative temperature change between the apparent and real temperatures. To this end, we
 225 discuss the N/Z asymmetry dependence of ΔT using model simulations in the following
 226 subsection. Once we deduce the relation of ΔT vs source N/Z asymmetry, the N/Z asym-
 227 metry dependence of the real source temperature can be inferred from those of the apparent
 228 temperature and ΔT . A similar analysis procedure has already been applied to study the
 229 source N/Z asymmetry dependence of the nuclear caloric curve with the double isotope ratio
 230 thermometers by Sfienti *et al.* [5].

231 **2. QUALITATIVE SEQUENTIAL DECAY EFFECT ON N/Z ASYMMETRY DE-** 232 **PENDENCE OF NUCLEAR TEMPERATURE**

233 To model the fragmentation process, a number of theoretical models have been developed
 234 in two distinct scenarios. One scenario is based on transport theory in which nucleon propa-
 235 gation in a mean field and nucleon-nucleon collisions under Pauli-blocking are the two main
 236 physical processes. The other scenario assumes that the fragmentation takes place in equi-
 237 librated nuclear matter and the break-up configuration determined by statistical weights.

238 We employ models for both scenarios, AMD used in the above sections and the statistical
 239 multifragmentation model (SMM) of Bondorf *et al.* [44]. For both calculations, the primary
 240 fragments are commonly identified as those directly from the fragmentation processes, and
 241 the secondary fragments are then generated using an afterburner. Different afterburners are
 242 employed in these two calculations. The GEMINI code of Charity *et al.* [37] is coupled with
 243 the AMD simulations, whereas the default encapsulated sequential decay code is used in
 244 SMM simulations. The system N/Z asymmetry in the AMD+GEMINI calculations, δ_{system} ,
 245 and source N/Z asymmetry in the SMM calculations, δ_{source} , are adopted to quantize the
 246 “source” N/Z asymmetry, δ , for a simplification. Note again that in the following analysis,
 247 the relative temperature change, ΔT , is defined as the difference between the temperatures
 248 from the secondary and primary isotope yields.

249 For the AMD+GEMINI analysis, the $^{58}\text{Ti} + ^{58}\text{Ti}$, $^{58}\text{Fe} + ^{58}\text{Fe}$ and $^{58}\text{Ni} + ^{58}\text{Ni}$ reaction
 250 systems at 40 MeV/nucleon are simulated. The lighter systems are chosen to mitigate the
 251 heavy CPU demand of the AMD simulations. The AMD simulations are performed with the
 252 Gogny interaction [45] and the Li-Machleidt in-medium nucleon-nucleon cross sections [46].
 253 IMFs are identified at 300 fm/c using a coalescence technique with the radius of $R_c = 5$ in
 254 phase space and then transferred to GEMINI for de-excitations. Inclusive IMFs are used to
 255 calculate the yields from an impact parameter range of 0-8 fm. The resultant ΔT values as a
 256 function of δ are shown in Fig. 8. Errors are evaluated in the same way as in the data shown
 257 in of Fig. 5. The global linear fit is also applied to the resultant AMD+GEMINI ΔT values.
 258 A weak dependence of ΔT on the source N/Z asymmetry is observed, although the absolute
 259 ΔT values fluctuate for the different thermometers. This can be attributed to the fact that
 260 the nuclear structure characteristics in the secondary decay process is the same for a given
 261 double isotope ratio selection among the reaction systems with different N/Z asymmetry,
 262 even if they are not fully taken into account. A common slope, $k_{\Delta T}^{AMD} = -1.9 \pm 0.5$ MeV,
 263 is obtained from the fit. The negative sign of $k_{\Delta T}^{AMD}$ is the same to that of the experimental
 264 value, k_{app} from Fig. 5. The absolute value of $k_{\Delta T}^{AMD}$ is nearly four times larger than that
 265 of k_{app} , but is still rather small, suggesting a weak N/Z asymmetry dependence of ΔT in
 266 the present AMD+GEMINI analysis. This $k_{\Delta T}^{AMD}$ value has a consistent magnitude with
 267 the deduced $|k_{\Delta T}| \lesssim 2.5$ MeV from the previous observation reported by Sfienti *et al.* [5],
 268 in which the deviation of the secondary decay corrections is smaller than 300 keV as the
 269 projectile-like fragmenting source changes among ^{107}Sn , ^{124}La and ^{124}Sn .

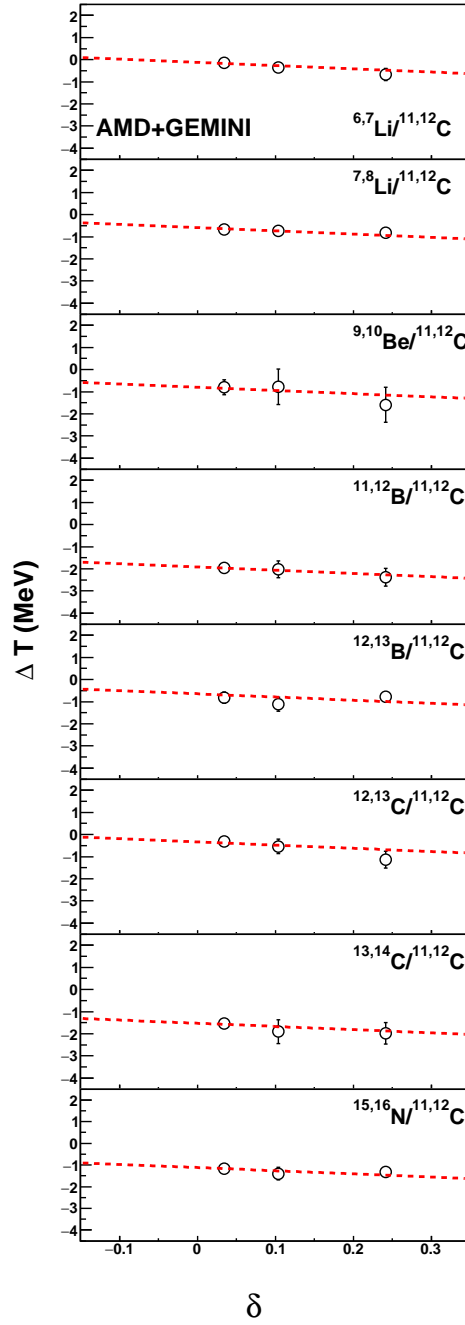


FIG. 8. (color online) Temperature difference ΔT between the temperatures from the secondary and primary isotope yields from the AMD+GEMINI simulations determined using the eight carbon-related thermometers as a function of δ . Red dashed lines represent the global fits with linear functions with one common slope $k_{\Delta T}^{AMD}$ and different intercepts.

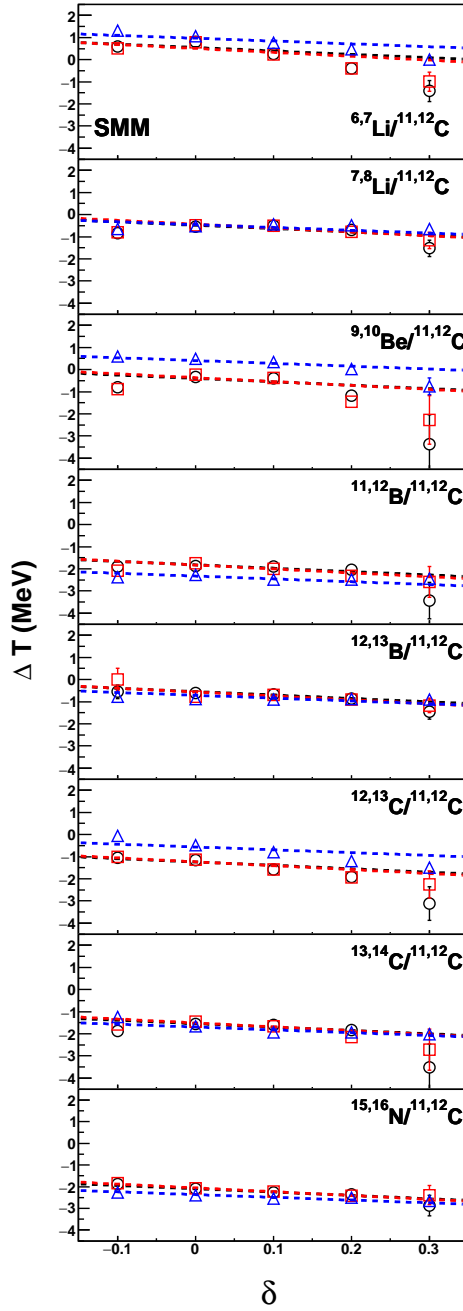


FIG. 9. (color online) Temperature difference ΔT between the temperatures from the secondary and primary isotope yields from the SMM simulations determined using the eight carbon-related thermometers as a function of δ . Initial fragmentation conditions are $E_x = 5$ MeV/nucleon and $\rho/\rho_0 = 0.1$ (circles), $E_x = 5$ MeV/nucleon and $\rho/\rho_0 = 0.2$ (squares), $E_x = 10$ MeV/nucleon and $\rho/\rho_0 = 0.2$ (triangles). Dashed lines represent the corresponding global fits with linear functions with one common slope $k_{\Delta T}^{SMM}$ and different intercepts.

271 SMM is also utilized to simulate the fragmentation of $A = 100$ sources with different Z
 272 numbers, i.e., $Z = 35, 40, 45$ and 55 . The fragmentation conditions are specified as excita-
 273 tion energies $E_x = 5-10$ MeV/nucleon and breakup densities $\rho/\rho_0 = 0.1-0.2$. The selection of
 274 $E_x = 5-10$ MeV/nucleon corresponds to the temperature range of $5-7$ MeV examined in our
 275 previous work [47] and covers the temperature region which has been previously extracted
 276 from the IMF yields of the reaction $^{64}\text{Zn} + ^{112}\text{Sn}$ at 40 MeV/nucleon using a self-consistent
 277 method. In Fig. 9, the resultant ΔT vs δ relations under different initial fragmentation con-
 278 ditions are plotted for $E_x = 5$ MeV/nucleon and $\rho/\rho_0 = 0.1$ (circles), $E_x = 5$ MeV/nucleon
 279 and $\rho/\rho_0 = 0.2$ (squares) and $E_x = 10$ MeV/nucleon and $\rho/\rho_0 = 0.2$ (triangles). For the
 280 results under a given condition, the same global fit is applied, and three common slope
 281 values are obtained as $k_{\Delta T}^{\text{SMM}} = -1.5 \pm 0.2$ MeV, -1.8 ± 0.2 MeV and -1.3 ± 0.2 MeV,
 282 respectively. The consistency of these slope values strongly suggests a consistency of the
 283 N/Z asymmetry dependence of the sequential ΔT due to decay for source excitation energies
 284 and breakup densities. These slope values are also in rather good agreement with that of
 285 AMD+GEMINI, although AMD and SMM follow completely different fragmentation pro-
 286 cesses. It further confirms the weak dependence of the relative temperature change on the
 287 source N/Z asymmetry.

288 Combining the results in this section to the determined weak N/Z asymmetry dependence
 289 of the apparent temperature from the experimental IMF yields in the previous section, it can
 290 be inferred that the N/Z asymmetry dependence of the real source temperature from IMFs is
 291 very small. In the theoretical work of Refs. [48, 49], Kolomietz *et al.* proposed that, a weak
 292 N/Z asymmetry dependence of temperature close to the phase transition appears under
 293 an equilibrium at a low pressure of $p = 10^{-2}$ MeV/fm³ within the thermal Thomas-Fermi
 294 approximation. Similar conclusion was also reached by Hoel *et al.* [9]. Combining these
 295 theoretical predictions, the obtained weak N/Z asymmetry dependence of the real source
 296 temperature from IMFs favors a physical picture that IMFs are generated in a low-pressure
 297 configuration via a “soft” expansion.

298 3. COMPARISON WITH THOSE FROM OTHER WORK

299 In the following, we compare our results with those from other published work. We begin
 300 by describing and discussing the details of the experimental works.

301 1. Kunde *et al.* [30] measured LCPs (d, t, ^3He , ^4He) from central collisions ($b/b_{max} < 0.3$)
302 of $^{124}\text{Sn} + ^{124}\text{Sn}$ and $^{112}\text{Sn} + ^{112}\text{Sn}$ at 40 MeV/nucleon with 280 plastic scintillator detectors
303 of the Miniball/Miniwall array mounted in the Superball scattering chamber. The double
304 isotope ratio thermometer with $^2,^3\text{H}/^3,^4\text{He}$ was employed. No correction for the sequential
305 decay effect was made.

306 2. Sfienti *et al.* [5] and Trautmann *et al.* [6] took measured particles from the projectile
307 fragmentations of ^{124}Sn , ^{124}La and ^{107}Sn on ^{nat}Sn at 600 MeV/nucleon as a probe. Charged
308 particles were measured with the ALADIN forward spectrometer at SIS, GSI Darmstadt.
309 Double isotope ratio thermometers with $^{6,7}\text{Li}/^3,^4\text{He}$ and $^{9,7}\text{Be}/^8,^6\text{Li}$ were utilized. The se-
310 quential decay effects were considered.

311 3. McIntosh *et al.* [8] studied the N/Z asymmetry dependence of the nuclear caloric curve
312 with the LCPs from the projectile fragmentation of $^{70}\text{Zn} + ^{70}\text{Zn}$, $^{64}\text{Zn} + ^{64}\text{Zn}$ and $^{58}\text{Ni} + ^{58}\text{Ni}$
313 at 35 MeV/nucleon. Both charged particles and associated neutrons were measured with
314 the NIMROD-ISiS 4π detector array [50]. Excitation energies were determined from the
315 reconstructed quasi-projectiles for noncentral collisions. The classical quadrupole momen-
316 tum fluctuation thermometer [8] with protons was used to extract the temperature. No
317 corrections for secondary decays was made with an assumption of a negligible contribution
318 of the thermal energy in the primary clusters to the width of the quadrupole momentum [8].

319 Among above experiments, a negligible N/Z asymmetry dependence of the apparent
320 temperature was observed by Kunde *et al.* and Sfienti *et al.*, in a good agreement with
321 our present result. Sfienti *et al.*, as mentioned above, further pursued the dependence of
322 secondary decay corrections on the source N/Z asymmetry, and found no significant N/Z
323 asymmetry effects greater than 300 keV [5]. A negligible N/Z asymmetry dependence of
324 the real source temperature was therefore concluded. This conclusion has been used as
325 experimental support for the assumption of N/Z asymmetry independence of the source
326 temperature when the symmetry energy was extracted from isoscaling [51, 52]. Different
327 isotope ratios of LCPs and IMFs were used in the analysis procedures of Sfienti *et al.* and
328 those of this work, but a consistent negligible N/Z asymmetry dependence of the source
329 temperature is observed. This fact is an indication at early chemical equilibrium prior to
330 the source fragmentation, since LCPs and IMFs involve different emission time scales in the
331 collisions [53, 54]

332 The temperatures evaluated by McIntosh *et al.* [8] show a notable decreasing trend as the

333 source N/Z asymmetry increases, that is, the extracted quadrupole momentum fluctuation
 334 temperature values with protons are well described by a linear fit over the broad range of
 335 the source N/Z asymmetry with a slope of -7.3 MeV, independent of the source excitation
 336 energies [31]. The quadrupole momentum fluctuation temperature with heavier isotopes
 337 show even larger slopes [31], -14.6 MeV slope for ${}^9\text{Be}$ for instance. However, it should
 338 also be mentioned that an earlier measurement of the same group with ${}^{86,78}\text{Kr} + {}^{64,58}\text{Ni}$ at
 339 35 MeV/nucleon was performed by Wuenschel *et al.* [7], and the obtained temperatures do
 340 not show a significant N/Z asymmetry dependence as those obtained by McIntosh *et al.* in
 341 Refs. [8, 31], where the same quadrupole momentum fluctuation thermometers were applied.
 342 In Ref. [31], they pointed out that the absence of the N/Z asymmetry dependence of the
 343 temperature is due to the inaccurate quasi-projectile source selection in the experiment of
 344 Wuenschel *et al.* [8], and that if the quasi-projectile sources are selected properly, a similar
 345 result is expected. Later, McIntosh *et al.* also applied the double isotope ratio thermometers
 346 (${}^{2,3}\text{H}/{}^{3,4}\text{He}$ and ${}^{6,7}\text{Li}/{}^{3,4}\text{He}$) to the same data set [31]. In contrast to those from quadrupole
 347 momentum fluctuation thermometers, the extracted apparent temperatures become much
 348 less dependent on the source N/Z asymmetry with a absolute slope value smaller than -1
 349 MeV, in good agreement with our present results.

350 VI. SUMMARY

351 The N/Z asymmetry dependence of the nuclear temperature is experimentally investi-
 352 gated with the IMF isotopes produced from 13 reaction systems with different N/Z asym-
 353 metries, ${}^{64}\text{Zn}$ on ${}^{112}\text{Sn}$ and ${}^{70}\text{Zn}$, ${}^{64}\text{Ni}$ on ${}^{112,124}\text{Sn}$, ${}^{58,64}\text{Ni}$, ${}^{197}\text{Au}$, ${}^{232}\text{Th}$ at 40 MeV/nucleon.
 354 The apparent temperatures for these systems are determined from the measured IMFs yields
 355 from the IV sources using eight carbon-related double isotope ratio thermometers. A rather
 356 negligible N/Z asymmetry dependence of the extracted apparent temperature is observed in
 357 the N/Z asymmetry range from 0.14 to 0.27 . In order to take into account the alteration of
 358 the measured isotope yields by sequential decay, the N/Z asymmetry dependence of the rel-
 359 ative temperature change, which is defined as the difference between the temperatures from
 360 secondary and primary isotope yields, is investigated using the AMD+GEMINI and SMM
 361 simulations. The real source temperature is then qualitatively inferred to have a rather weak
 362 dependence on the source N/Z asymmetry. The present result is compared with those from

363 other independent experiments. It is found that the temperature deduced from the double
364 isotope ratio thermometers commonly shows a small N/Z asymmetry dependence, consis-
365 tent with results using thermometers with LCPs and IMFs. In contrast, the temperature
366 in another experiment deduced from the quadrupole momentum fluctuation thermometers
367 shows a significant decrease with increasing the source N/Z asymmetry.

368 ACKNOWLEDGEMENT

369 The authors thank the operational staff in the cyclotron Institute, Texas A&M University,
370 for their support during the experiment. The authors thank A. Ono for providing his
371 code. This work is supported by the National Natural Science Foundation of China (No.
372 11705242, 11805138, 11775273, 11575269), the Fundamental Research Funds For the Central
373 Universities (No. YJ201954, YJ201820 and GK201903022) in China, the CAS Pioneer
374 Hundred Talents Program and the National MCF Energy R&D Program of China (No.
375 2018YFE0310200). This work is also supported by the US Department of Energy under
376 Grant No. DE-FG02-93ER40773 and the Robert A. Welch Foundation under Grant A330.

-
- 377 [1] W. A. Friedman, Phys. Rev. Lett. **60**, 2125 (1988).
378 [2] E. Suraud, C. Gregoire, and B. Tamain, Prog. Part. Nucl. Phys. **23**, 357 (1989).
379 [3] D. Gross *et al.*, Prog. Part. Nucl. Phys. **30**, 155 (1993).
380 [4] Bao-An Li, Lie-Wen Chen, and Che Ming Ko, Phys. Rep. **464**, 113 (2008).
381 [5] C. Sfienti *et al.*, Phys. Rev. Lett. **102**, 152701 (2009).
382 [6] W. Trautmann *et al.*, Int. J. Mod. Phys. **E 17**, 1838 (2008).
383 [7] S. Wuenschel *et al.*, Nucl. Phys. **A 843**, 1 (2010).
384 [8] A.B. McIntosh *et al.*, Phys. Lett. **B 719**, 337 (2013).
385 [9] C. Hoel, L.G. Sobotka, R.J. Charity, Phys. Rev. **C 75**, 017601 (2007).
386 [10] J. Besprosvany, S. Levit, Phys. Lett. **B 217**, 1 (1989).
387 [11] R. Ogul, A.S. Botvina, Phys. Rev. **C 66**, 051601 (2002)(R).
388 [12] J. Su, F.S. Zhang, Phys. Rev. **C 84**, 037601 (2011).
389 [13] F. Zhang *et al.*, Phys. Rev. **C 91**, 034617 (2015).

- 390 [14] T.X. Liu *et al.*, Euro. phys. Lett. **74**, 806 (2006).
- 391 [15] W.A. Friedman and W.G. Lynch, Phys. Rev. **C 28**, 16 (1983).
- 392 [16] S.R. Souza and R. Donangelo, Phys. Rev. **C 97**, 054619 (2018).
- 393 [17] J.B. Natowitz *et al.*, Phys. Rev. **C 65**, 034618 (2002).
- 394 [18] B. Borderie and M. F. Rivet, Prog. Part. Nucl. Phys. **61**, 551 (2008).
- 395 [19] W. Lin *et al.*, Phys. Rev. **C 89**, 021601 (2014)(R).
- 396 [20] W. Lin *et al.*, Phys. Rev. **C 90**, 044603 (2014).
- 397 [21] X. Liu *et al.*, Phys. Rev. **C 90**, 014605 (2014).
- 398 [22] X. Liu *et al.*, Nucl. Phys. **A 933**, 290 (2015).
- 399 [23] X. Liu *et al.*, Phys. Rev. **C 97**, 044603 (2018).
- 400 [24] X. Liu *et al.*, Phys. Rev. **C 92**, 014623 (2015).
- 401 [25] S. Albergo *et al.* Nuovo Cimento **A 89**, 1, (1985).
- 402 [26] W. Trautmann *et al.*, Phys. Rev. **C 76**, 064606 (2007).
- 403 [27] H.F. Xi, W.G. Lynch, and M.B. Tsang, Phys. Rev. **C 59**, 1567 (1999).
- 404 [28] H.F. Xi *et al.*, Phys. Rev. **C 58**, 2636 (1998) (R).
- 405 [29] V. Serfling *et al.*, Phys. Rev. Lett. **80**, 3928 (1998).
- 406 [30] G.J. Kunde *et al.*, Phys. Lett **B 416**, 56 (1998).
- 407 [31] A.B. McIntosh *et al.*, Eur. Phys. J. **A 50**, 35 (2014).
- 408 [32] J. Wang *et al.*, Phys.Rev. **C 72**, 024603 (2005).
- 409 [33] F. Hubert, R. Bimbot, and H. Gauvin, At. Data Nucl. Data Tables **46**, 1 (1990).
- 410 [34] I. Tilquin *et al.*, Nucl. Instrum. Methods **A 365**, 446 (1995).
- 411 [35] M. Huang *et al.*, Phys.Rev. **C 88**, 034605 (2013).
- 412 [36] A. Ono, Phys. Rev. **C 59**, 853 (1999).
- 413 [37] R.J. Charity *et al.*, Nucl. Phys. **A 483**, 371 (1988).
- 414 [38] R. Wada *et al.*, Phys. Rev. **C 69**, 044610 (2004).
- 415 [39] M. Huang *et al.*, Phys.Rev. **C 82**, 054602 (2010).
- 416 [40] T.C. Awes, G. Poggi, C.K. Gelbke *et al.*, Phys. Rev. **C 24**, 89 (1981).
- 417 [41] Z. Chen *et al.*, Phys.Rev. **C 81**, 064613 (2010).
- 418 [42] M.B. Tsang, W.G. Lynch and H. Xi, Phys. Rev. Lett. **78**, 3836 (1997).
- 419 [43] S. Das Gupta, A.Z. Mekjian, M. B. Tsang, Advances in Nuclear Physics, pp 89-166 (2001),
420 Boston US.

- 421 [44] J. Bondorf, A. S. Botvina, A. S. Iljinov, I. N. Mishutin, and K. Sneppen, Phys. Rep. **257**, 133
422 (1995).
- 423 [45] A. Ono and H. Horiuchi, Prog. Part. Nucl. Phys. **53**, 501 (2004).
- 424 [46] G.Q. Li, R. Macheliedt, Phys. Rev. **C 49**, 566 (1994).
- 425 [47] W. Lin *et al.*, Phys. Rev. **C 99**, 054616 (2019).
- 426 [48] V.M. Kolomietz *et al.*, Phys. Rev. **C 64**, 024315 (2001).
- 427 [49] S. Shlomo and V.M. Kolomietz, Rep. Prog. Phys. **68**, 1 (2005).
- 428 [50] S. Wuenschel *et al.*, Nucl. Instrum. Methods Phys. Res. **A604**, 578 (2009).
- 429 [51] H.S. Xu *et al.*, Phys. Rev. Lett. **85**, 716 (2000).
- 430 [52] M.B. Tsang *et al.*, Phys. Rev. **C 64**, 054615 (2001).
- 431 [53] F.Z. Ighezou *et al.*, Nucl. Phys. **A 662**, 295 (2000).
- 432 [54] N. Buyukcizmeci *et al.*, Phys. Rev. Lett. **84**, 5971 (2000).